

1 Source location and wavefield characterization of river-induced 2 seismic tremor

3
4 Haleh Karbala Ali¹ and Christopher J. Bean¹

5 ¹Geophysics Section, School of Cosmic Physics, Dublin Institute for Advanced Studies, Dublin, Ireland.

6 *Correspondence to:* Haleh Karbala Ali (haleh@cp.dias.ie)

7 **Please note that this is the version 2 of a preprint listed on EarthArXiv prepared for submission to Earth**
8 **Surface Dynamics which has not undergone full peer review yet. Subsequent versions may have slightly**
9 **different content. Please contact the first author for any question or feedback regarding this work.**

10
11 **Abstract.** River-induced seismic signal (tremor) recorded by deploying seismic stations close to the river can be used
12 to obtain the flow characteristics of rivers indirectly. This task becomes challenging when the tremor is contaminated
13 by strong cultural noise. We conducted an experiment next to Avoca River, County Wicklow, Ireland. We locate and
14 characterize the river-induced tremor by combining the application of beamforming array analysis, by deploying two
15 seismic arrays, and Frequency-Dependent Polarization Analysis (FDPA) via the deployment of a few single three-
16 component seismometers at different offsets from the river. FDPA on single stations revealed that the tremor consists
17 of Rayleigh, Love, and body waves when it was distinguishable from mixed waves depending on the station's distance
18 from the river. Where Rayleigh waves dominated, we computed the single station back-azimuth (BAZ) of the tremor
19 which was in agreement with the BAZ obtained through array analysis. When wave types are not mixed, we observed
20 that the tremor signal recorded by the stations in the arrays is Love wave-dominated. It was also observed that at time
21 periods of strong cultural noise, the Rayleigh wave component of the tremor emanating from the river is enhanced,
22 suggesting the possibility that surface waves induced by cultural activities get trapped in the river. Moreover, the
23 observation of the correlation between the median filtered seismic power integrated within the frequency range of the
24 tremor and the river flow rate demonstrated the capability of passive seismic as an indirect hydraulic monitoring tool,
25 even in the presence of strong cultural noise.

26 Plain Language Summary

27 Turbulency of water flow and sediments carried in water courses are the leading causes that induce tiny ground
28 vibrations which cannot be sensed by humans even if standing close to the river. These micro-vibrations can however
29 be detected and monitored by sensitive seismic instruments placed adjacent to the river. Detection of these ground
30 vibrations becomes challenging when the river is near a construction site, railway, local roads, and residential areas
31 as human activities also shake the ground. This study shows that we can infer the change in river flow rate based on

32 how the strength of these vibrations changes over time. Moreover, the details of the oscillation directions of the
33 vibrations may reveal the details of how the flowing water is interacting with the river bed.

34 **1 Introduction**

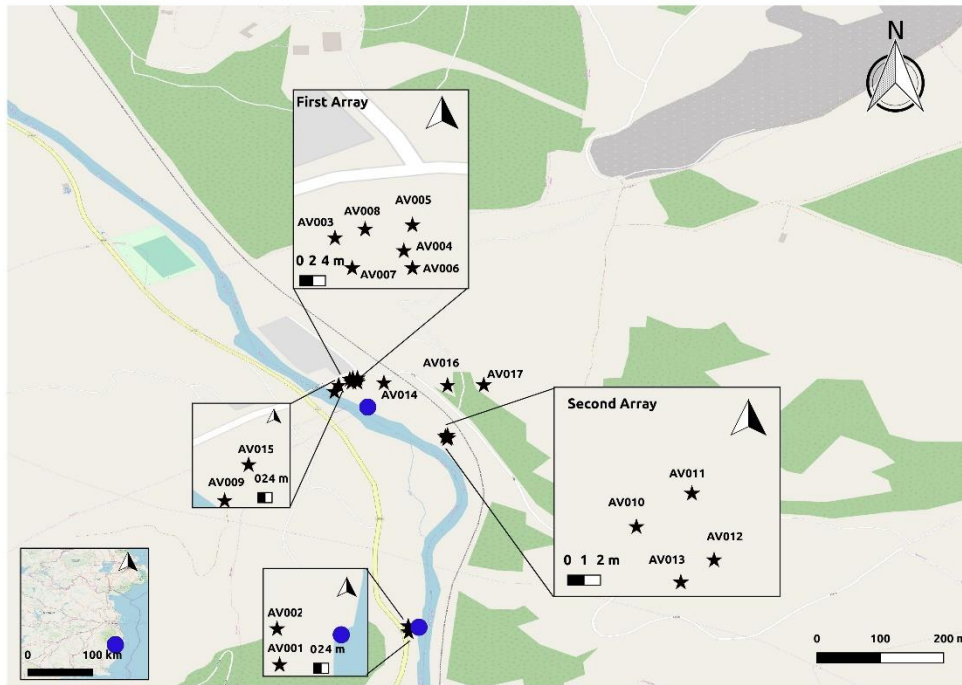
35 Different hydraulic processes in surface rivers induce tiny ground vibrations (in the range of nano- to micro-meters)
36 which can be identified by deploying sensitive seismic stations near a river. These processes include turbulent water
37 flow, bed-load transport, air bubbles explosion, and the generation of gravity or breaking waves at the river surface
38 (Schmandt et al., 2013, Laros et al., 2015). Govi et al. (1993) were the first to report the change in seismic signal
39 amplitude due to variation in discharge conditions. Huang et al. (2007) explored the origins of ground vibrations
40 caused by debris flows. Burtin et al. (2008, 2011) explored the use of seismic noise produced by rivers to monitor the
41 bed load transport for the trans-Himalayan Trisuli river and the low-discharge Torrent de Saint Pierre braided river in
42 the French Alps, respectively. Burtin et al. (2010) located the Trisuli river-induced seismic signal using noise
43 correlation functions. Winberry et al. (2009) reported the resonance of subglacial cracks and conduits containing
44 water as a sustained seismic tremor and could track and locate the tremor using array analysis. Tsai et al. (2012)
45 developed the first forward model describing the power spectral density of Rayleigh waves generated through the
46 impacts of grains on the river bed. Gimbert et al. (2014) introduced a mechanistic model describing the seismic noise
47 generation as a result of time-varying normal and shear stress of turbulent water- flow against the river bed. Gestrich
48 et al. (2020) developed a physical model for volcanic eruption tremor based on similarities in physical processes and
49 observed seismic tremor in rivers. Bartholomaeus et al. (2015) quantified the seasonal subglacial discharge based on
50 the tremor power. Schmandt et al. (2017) used a dense array along Trinity River in a dam-controlled and gravel
51 augmentation experiment to study the spatio-temporal extent of sediment transport. Anthony et al. (2018) observed
52 a low-frequency signal sensitive to discharge dominant on horizontal components of stations within 1 m of the channel
53 boundary as a result of sensor tilt due to viscoelastic deformation in the hyperheic zone. Goodling et al. (2018) studied
54 the dam spillway monitoring based on Frequency-Dependent Polarization Analysis (FDPA) to locate the turbulence
55 flow and characterize the surface waves induced by dam floods. Vore et al. (2019) studied the subglacial water systems
56 using FDPA to distinguish between single and multi-conduit flow paths and characterization of the seismic tremor.
57 Coviello et al. (2019) proposed a debris flow detection algorithm based on the amplitude information gathered from
58 a linear array of geophones installed along the channel in an early warning system. Eibl et al. (2020) located and
59 tracked the subglacial flood front based on array analysis of the seismic tremor and reported early warning capability.
60 To our knowledge, the study we report herein combines, for the first time, the application of array processing using
61 clusters of seismic stations and Frequency-Dependent Polarization Analysis (FDPA) based on single three-component
62 seismic stations to locate river-induced seismic tremor and characterize tremor wave-type composition. Here we
63 observed different wave components within river-induced tremor and showed that Love waves are more prevalent
64 than Rayleigh waves. We also observed the enhancement in Rayleigh wave composition after 5:00 A.M. which can
65 be attributed to noise induced by daily cultural activities trapped in the river. Finally, the correlation observed between
66 flow-rate and river-induced tremor, despite the extensive amount of cultural noise, confirmed the applicability of
67 fluvial seismology for monitoring rivers in urban settings and in areas with strong cultural noise.

68 **2 Methods**

69 **2.1 Research Site and Instrumentation**

70 We conducted the experiment between 10th-15th October 2019 next to Avoca River, County Wicklow, Ireland. The
71 main reason for choosing this site for the experiment was the existence of permanent monitoring flow-gauges
72 belonging to the Environmental Protection Agency (EPA). This enabled us to investigate the correlation between
73 water-level/flow-rate change, with change in seismic signature induced by the river. The study site located close to
74 the Wicklow County Council construction site, a railway line, and local road, therefore the data were highly
75 contaminated by cultural noise. We used three-components (3C) Lennartz short-period 1Hz seismometers and data-
76 cube digitizers with a sampling frequency of 200 Hz. We deployed stations AV001- AV013 on October 10th and
77 stations AV014- AV017 on October 14th and retrieved them on October 15th 2019. We deployed two seismic arrays,
78 up-and down-stream of the river, each consisting of 6 and 4 stations, respectively. When a cluster of seismic stations
79 is deployed together they constitute a seismic array. With an array, we can improve the signal-to-noise ratio (SNR) by
80 summing the coherent signals from the single array stations. We deployed station AV009 close to the river where the
81 flow gauge was mounted to investigate the correlation between flow-rate/water-level data from the flow gauge and
82 the river-induced seismic signal until December 18th 2019. Figure 1 shows the location map of the Avoca River, the
83 deployed seismic stations and arrays, and the EPA flow gauges. To alleviate the effect of noise on seismic data we
84 buried all seismic sensors in 30cm-deep pits. Figure 2 shows the seismometer, data-logger, and deployment in the
85 field.

86
87
88
89
90
91
92
93
94
95
96
97
98
99
100
101
102
103
104
105
106



107 **Figure 1: The location map of the experiment next to the Avoca River, County Wicklow, Ireland between 10th- 15th October**
108 **2019. The deployed seismic stations and the EPA flow-gauges are shown as stars and blue circles, respectively.**

109
110
111
112
113
114
115
116
117
118
119
120
121



Figure 2: Seismic instruments used throughout the fieldwork. (a) Three-component (3C) Lennartz short-period 1Hz seismometer, data-cube digitizer and breakout-box to connect seismometer with the data-logger, (b) deployment of the seismometer in a 30cm deep pit to alleviate the effect of cultural noise.

122 2.2 Beamforming Array-processing

123 The river-induced seismic tremor has no definite onset, so we cannot use conventional earthquake location methods
124 based on P- and S-wave arrivals to determine the direction of arrival of the seismic signals. However, by deploying a
125 group of stations as an array, we could apply frequency-wavenumber (F-K) analysis to simultaneously determine the
126 back-azimuth (BAZ), i.e., the direction of arrival of the wavefront measured with respect to the North, and the
127 slowness, i.e., the inverse of wave speed. For the joint determination of back-azimuth and slowness of a wave, both
128 frequency-domain methods and time-domain methods exist. Here, we performed a frequency wavenumber (FK)
129 analysis with a moving time window. The FK analysis is a beamforming method in the spectral domain that performs
130 a grid search within a horizontal slowness grid (s_x and s_y). In each time window, the covariances of the Fourier
131 Transformed signal at each receiver pair are calculated. Phase delays of each plane wave described by the horizontal
132 slowness grid are applied and the trace of the resulting covariance matrix is the cross-spectral density. This is
133 undertaken for every grid point and results in absolute power and semblance maps (ratio of the averaged power of the
134 stacked trace and the stack of the average single trace powers) in the spectral domain with respect to the horizontal
135 slownesses. The maximum value in these maps is determined and converted to back-azimuth and slowness of the
136 incoming wave using the angle and length of the vector from the origin to the maximum, respectively. The underlying
137 assumptions include a plane wavefront, coherent signal and incoherent noise (Eibl et al., 2017). The array processing
138 output is a time-series of BAZ, slowness, absolute, and relative power (semblance). The dominant BAZ for each array
139 is the maximum of BAZ histogram and the dominant slowness value is the median of the slowness time-series.

140 2.3 Frequency-Dependent Polarization Analysis

141 Frequency-Dependent Polarization Analysis (FDPA) originally introduced by Park (1987) can be used to determine
142 different wave components such as Rayleigh, Love and body waves in the tremor and determine the BAZ of the
143 arriving waves when Rayleigh waves dominate. In this study, we applied the method described by Vore et al. (2019).
144 For the 3C seismic data at each station, we divided the signal into 60-second-long windows with a 50% overlap. After
145 applying the Fourier Transform to each component, the covariance spectral matrix for each frequency component is
146 calculated. An average spectral covariance matrix is then computed by linearly averaging the real and imaginary parts

147 of 7-minute binned data to eliminate short-transients. The polarization vector can be defined when the ground motion
148 is mostly constrained within a single plane of motion when the first singular value of the average spectral covariance
149 matrix is larger than the other two. We set the threshold value to 2. The wave composition of the tremor can be
150 identified based on the phase-lag between the vertical and horizontal components. If the phase-lag is between 0-20
151 degrees, either body or Love waves dominate the tremor with linear particle motion, whereas Rayleigh waves having
152 elliptical particle motion exhibit phase-lag between 70-90 degrees. Further differentiation between Love and body
153 waves is possible by comparing the power spectra of the vertical and horizontal components at each frequency. If the
154 magnitude of the horizontal power (average of the two horizontal components) is higher than the vertical one, the
155 signal is Love-wave dominated otherwise it consists mainly of body waves. The percentage of different wave types
156 for each frequency component is determined by choosing a 20% threshold. When Rayleigh waves dominate, it is
157 possible to determine the BAZ based on the amplitude ratio between horizontal components of the polarization vector.

158 **3 Data**

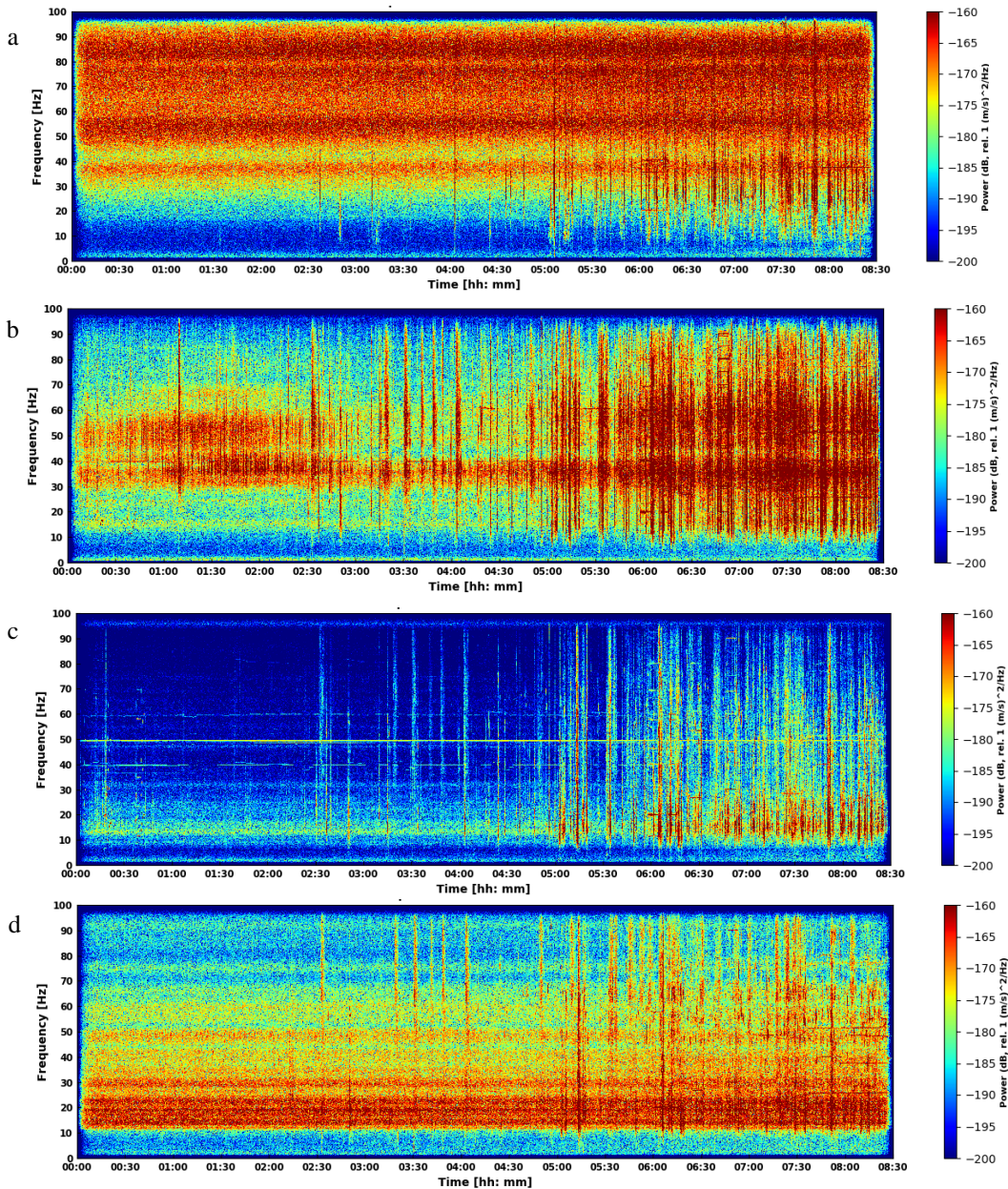
159 All the stations successfully recorded data for the whole deployment period. We removed the linear trend from the
160 data, tapered, and corrected for the instrument response. We applied a low-cut filter to remove microseism (signals
161 induced by ocean processes) which appeared quite strong in the low-frequency range below 3 Hz on our dataset. As
162 the river produces a continuous seismic source in time, the river-induced signal appears as a persistent frequency band
163 on spectrograms. In the following, we refer to the river-induced seismic signal as the tremor. We computed the
164 spectrograms of different stations with 8-second sliding windows of 50% overlap. Figure 3 shows the spectrogram of
165 the stations AV002, AV009, AV003, and AV011 on October 15th, 2019 from midnight to 08:30 A.M. We deployed
166 stations AV002 and AV009 very close to the river (<10m). Note the Station AV003 belongs to the first seismic array
167 deployed upstream 50m from the river and station AV011 is a representative from the second array deployed
168 downstream 30m from the river. We noticed the shift of the tremor persistent frequency band on spectrograms
169 depending on the seismic station offset to the river. The high frequencies get attenuated with distance from the river
170 as shown in the spectrogram of station AV003. Background cultural noise appears as vertical spikes on the
171 spectrograms. Note the cultural noise enhances from 5:00 A.M. which is the start of daily human activities. The
172 narrow-band signal at 50 Hz is induced by the electric power cables near the stations. The narrow band signals at 40
173 and 60 Hz are also stationary noise.

174 **4 Results**

175 Here we show the results of applying beamforming on October 15th, 2019 from midnight to 08:30 A.M. for the first
176 and second arrays. We bandpass filtered the seismic data in the discrete persistent frequency bands observed on the
177 spectrograms of the first array including 8-10, 10-14.26, and 19-22 Hz. The data set is divided into 60-second-long
178 time-windows with 50% overlap. In each of these windows, the standard FK analysis is performed. The result is a
179 time series of BAZ, horizontal slowness and relative power (semblance) of the predominant signal in each time

180 window. Changes in the BAZ suggest a source movement, while a change in slowness reveals different phases (wave
181 types) arriving at the array.

182
183
184
185
186
187
188
189
190
191



193
194
195
196
197
198
199
200
201
202

203
204
205
206
207
208
209
210
211

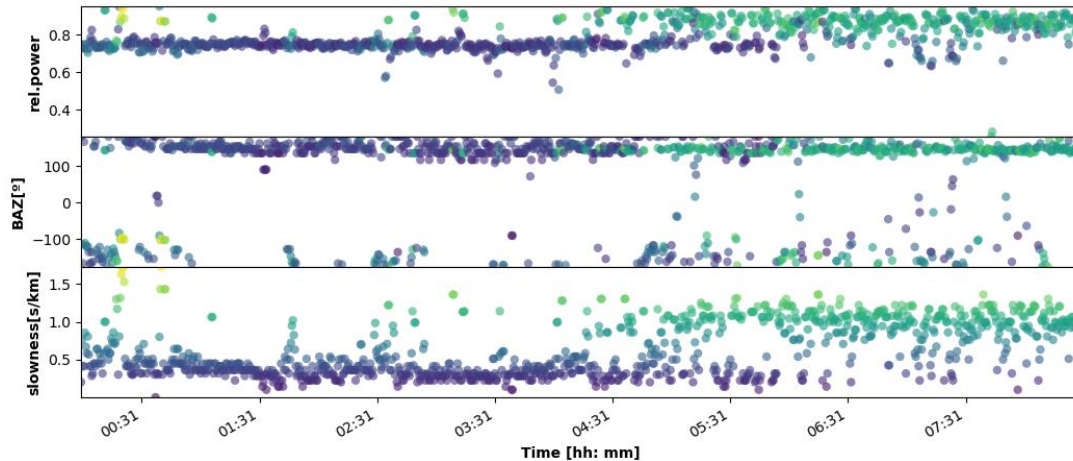
212
213
214
215
216
217
218
219
220
221

222 **Figure 3. (a-d): The spectrogram of stations AV002, AV009, AV003, and AV011 on October 15th 2019, respectively. The**
223 **frequency content of the tremor depends on the station's distance to the river. The noise-induced by cultural activity**
224 **appears as vertical spikes on the spectrograms. The cultural noise boost from 5:00 A.M. which is the start of daily human**
225 **activities.**

226
227
228
229
230

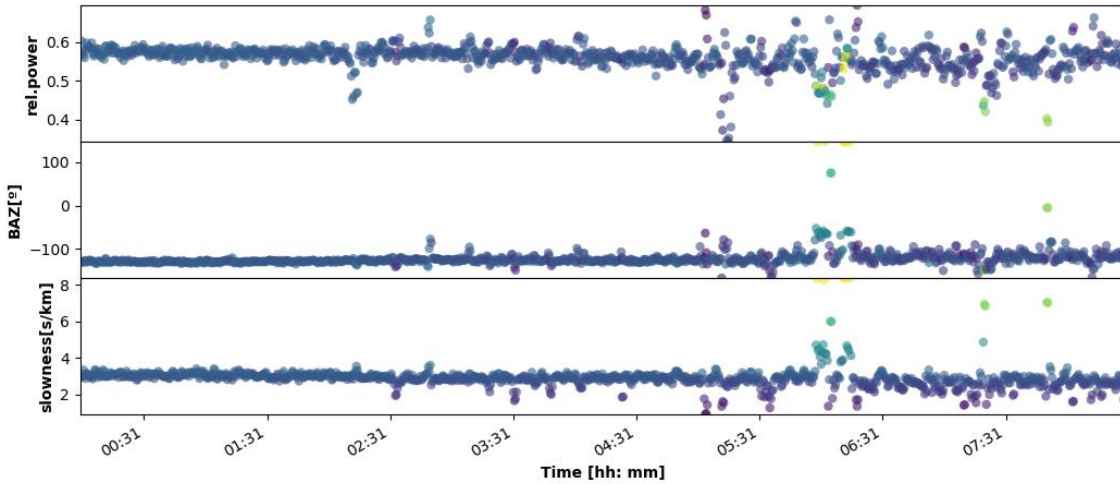
Figures S1-S5 in supplementary material demonstrate the result of beamforming for each discrete frequency band mentioned above. We noticed the tremor has a spectral signature in the frequency range 8-17 Hz as shown in Figure 4. The change in wave speed after 5:00 A.M. reflects the start of the daily human activities. In this case, the cultural noise has a similar BAZ as the river. Therefore, there is two possibilities: either the cultural noise is coming from the

231 same direction as the river or the cultural noise is amplified and trapped within the river. This is a hypothesis which
 232 needs further investigation. The persistent frequency in the range of 17-19 and 19-22 Hz are not river-induced. Note
 233 in Figures S4 and S5, the BAZ of the persistent non-river induced signal is different than the cultural noise that kicks
 234 in after 5:00 A.M.
 235



236 **Figure 4: Beamforming array-processing results for the first array in the frequency range 8-17 Hz** From top to bottom the
 237 time-series indicate semblance, absolute power, BAZ, and slowness. All panels are colour-coded based on slowness. The
 238 tremor shows a persistent BAZ as expected. Sudden changes in BAZ occur at a time of strong cultural noise. Note the
 239 change in wave speed after 5:00 A.M. when daily human activities start. This is also reflected in the enhanced relative power
 240 after 5:00 A.M.
 241

242
 243 We bandpass filtered the seismic data in the discrete frequency bands observed as persistent on the spectrograms of
 244 the second array including 10-14.65, 13-17, 21-23, 30-32 and 32-36 Hz, and applied the FK analysis similar to the
 245 first array. Figures S6-S12 in the supplementary material demonstrate the results of beamforming for each discrete
 246 frequency band mentioned above. We noticed that the tremor has a spectral signature in the frequency range 10-23 Hz
 247 as shown in Figure 5. The persistent frequency in the range 23-27, 27-30, 30-32 and 32-36 Hz are not river-induced
 248 as shown in Figures S9 to S12. Note that we don't observe any change in the slowness of the tremor after 5:00 A.M.
 249 for the second array compared to the first array. Our interpretation is that the second array is more distant to the source
 250 of the cultural noise, which is the local road in this case, compared to the first array as can be observed in Figure 1.



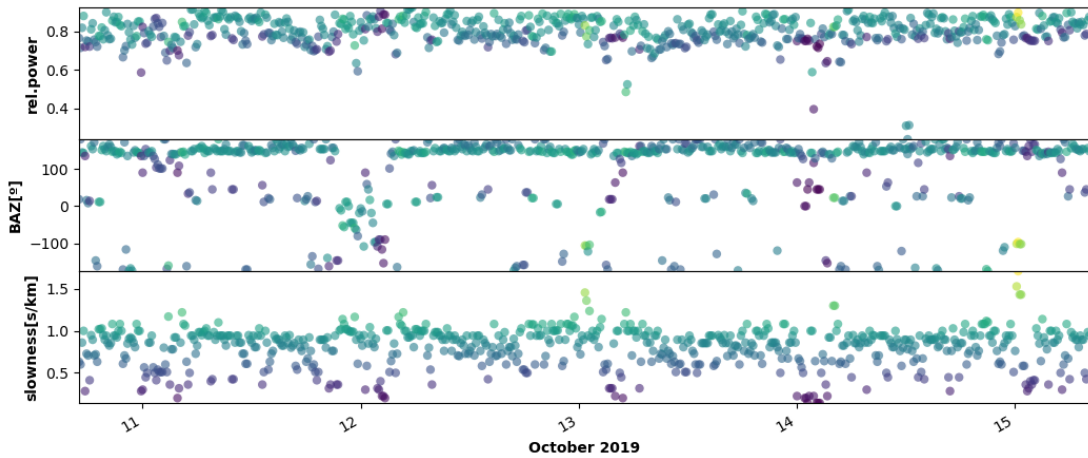
269

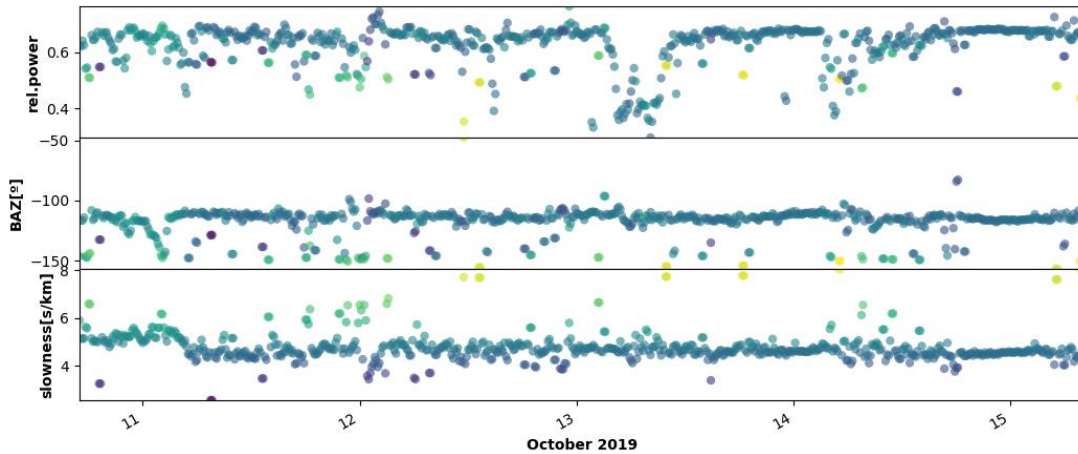
270 **Figure 5: Beamforming array-processing results for the second array in the frequency range 10-23 Hz. From top to bottom**
 271 **the time-series indicate semblance, absolute power, BAZ, and slowness. All panels are colour-coded based on slowness. The**
 272 **tremor shows a persistent BAZ as expected.**

273

274

275 Figure 6 shows the application of beamforming to the whole dataset between October 10th – October 15th 2019 with
 276 20 minutes window length of 50% overlap. Note that due to averaging, the effect of cultural noise is eliminated and
 277 the tremor shows up as persistent BAZ and slowness.





279
 280 **Figure 6: Beamforming array-processing results for the (top): first and (bottom): second array in the frequency range 8-17**
 281 **and 10-23 Hz, respectively for the whole data recording interval between 10th-15th October 2019. The window length of 20**
 282 **minutes with 50% overlap is used for FK analysis. Note the effect of cultural noise is eliminated due to longer window length**
 283 **and we observe a persistent BAZ and slowness for the river-induced signal. However, we still see change in BAZ and**
 284 **slowness during intervals of severe cultural noise.**
 285

286
 287 Two or more arrays are usually used to find the epicentral location of the source. We note the BAZs of the two arrays
 288 in our study do not coincide at a common point. Since seismic records at one station are sensitive to a broad portion
 289 of the river near it (Burtin et al., 2008) the array analysis tends to detect the strongest ‘point source’ closest to the
 290 array, while the river can be considered as a spatial series of many point sources, of varying strength, each array locates
 291 the strongest source, i.e., the strongest local point in the river, closest to it. Figure 7 depicts the BAZ of the tremor in
 292 the frequency range of 8-17 and 10-23 HZ for the first and second array, respectively.

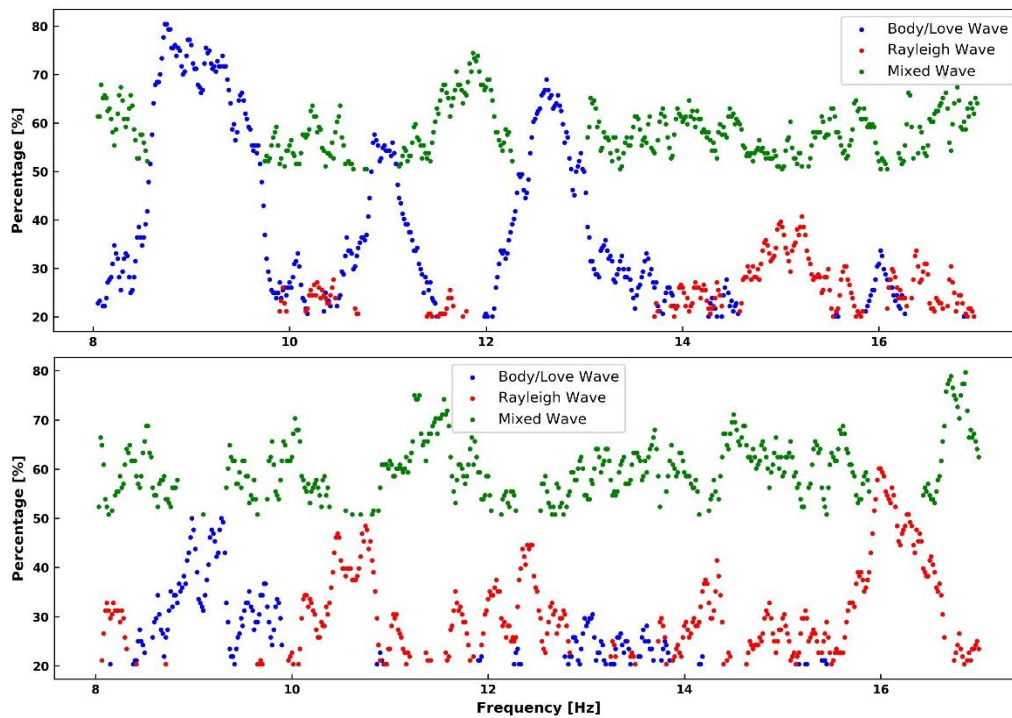
293
 294



295
 296
 297 **Figure 7: Determining the direction of arrival of the tremor to each array by calculating the BAZ based on beamforming.**
 298 **Each array locates the strongest closest point source. The yellow icons show the stations in each array and the red lines**
 299 **depict the BAZ, i.e., the direction of arrival of tremor in the frequency range of 8-17 and 10-23 Hz for the first and second**
 300 **array, respectively.**
 301

302 To further determine the wave composition of the tremor, we applied FDPA to data for the time interval between
 303 midnight to 5:00 A.M. and 5:00 A.M. to 8:30 A.M. as shown in Figures S13 and S14 in the supplementary material.
 304 The ratio between the first and second singular values of the spectral covariance matrix being above 2.5 was used to
 305 determine whether the signal is polarized or not. The wave type at each frequency is determined by applying a 20%
 306 threshold. To differentiate between body and Love waves, we looked at the power spectra of different components
 307 computed using the Welch method (Figure S15). When the horizontal powers are higher than the vertical one, the
 308 tremor is Love wave dominated. Figure 8 shows the wave percentage for these two time intervals for station AV003
 309 as the representative of the first array. Note that the highest percentage of the tremor is mixed waves at each frequency
 310 component. For the frequency range of 8-10 Hz Love waves dominate the remaining composition of the tremor for
 311 both of these time intervals. We did not observe any change in the slowness values of the tremor in these two time
 312 intervals for the frequency range 8-10 Hz (Figure S1). For the frequency range of 10-14 Hz, the tremor is Love wave
 313 dominated in the time interval midnight to 5:00 A.M while
 314 Rayleigh waves dominates in the interval 5:00 to 8:30 A.M. reflecting the beginning of human activities. This is
 315 consistent with the increase in the slowness values from array processing.

316



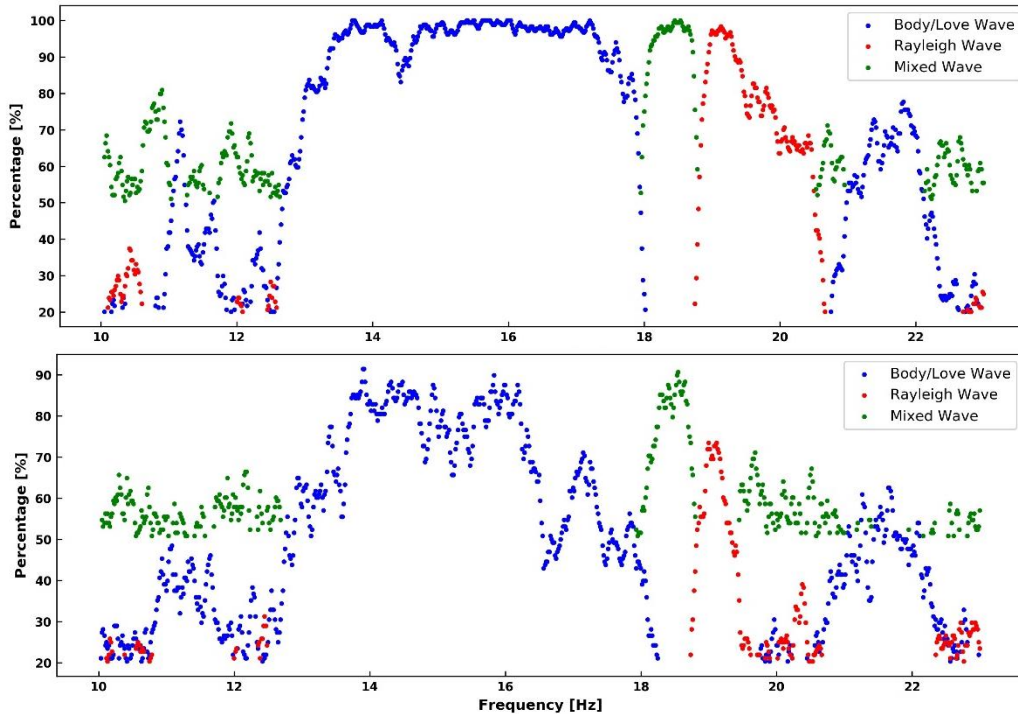
317

318

319 **Figure 8: The percentage of different wave types in the tremor in the frequency range 8-17 Hz for station AV003 as the**
 320 **representative of the first array. For the time interval (top) midnight to 5:00 A.M. and (bottom) 5:00 to 8:30 A.M. on**
 321 **October 15th 2019. Note when wave types are not mixed, Love waves dominate. Note the enhancement of Rayleigh wave**
 322 **composition of the tremor once the cultural noise increases after 5:00 A.M which is the start of daily human activity.**

323

324 Figure 9 shows the wave percentage for these two time intervals for station AV011 as the representative of the second
 325 array. Note the tremor consists mainly of Love waves. Moreover, the wave composition is similar for these two time
 326 intervals. This is consistent with the similar slowness values we obtained from array processing in these two time
 327 intervals.



328

329

330

331

332

333

334

335

336

337

338

339

340

341

342

343

344

345

346

347

348

349

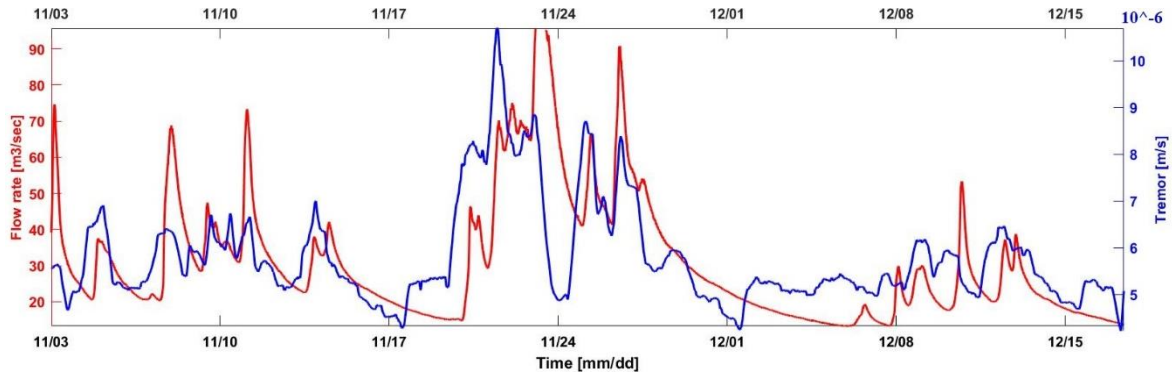
350

351

Figure 9: The percentage of different wave types in the tremor in the frequency range 10-23 Hz for station AV011 as a representative of the second array. For the time interval (top) midnight to 5:00 A.M. and (bottom) 5:00 to 8:30 A.M. on October 15th 2019. Note the tremor does not change in wave composition in these two time intervals.

As stated by Vore et al. (2019) to locate the tremor in a particular frequency range, three criteria need to be met. First, the power spectrum should show a peak in that frequency range. This is where we observed the persistent signals on the spectrograms in Figure 3. Second, the signal should be polarized, i.e., well-constrained particle motion and third is that Rayleigh waves dominate. The BAZ, computed based on the Rayleigh components of the tremor, for station AV003 and AV013 as the representatives of the first and second array is 150° and 235° , respectively. This is in agreement with the BAZ of 160° and 240° derived from array processing for these arrays. This shows FDPA using a single 3C seismic station is a promising tool in the absence of seismic arrays to locate river induced tremor when dominated by Rayleigh waves.

In the next step, we investigated the existence of correlation between the flow-rate recorded by the EPA flow-gauge and the seismic monitoring station, AV009, over the one and half months of deployment. Movie S1 in the supplementary material shows the spectrogram of the monitoring station AV009 between 10th October- 18th December 2019. Note the extent of cultural noise in the data. We computed median filtered spectrograms as proposed by Bartholomaus et al. (2015) to alleviate the effect of cultural noise on tremor amplitude. We then extracted the persistent signal in the frequency band between 11-14 Hz on the median-filtered spectrograms of the seismic monitoring station. The root mean square (RMS) of the sum of signal at each time sample in this frequency range yields a time series as shown in Figure 10. Note there is reasonably good correlation between the RMS signal and flow-rate, except for the time intervals with extensive cultural noise due to the construction site operating near the monitoring station.



352

353 **Figure 10: The correlation between the flow-rate and seismic tremor in the frequency range 11-14 Hz at the seismic**
 354 **monitoring station, AV009, Whitebridge, Co. Wicklow, Ireland between 10th October- 18th December 2019. This**
 355 **demonstrates the capability of fluvial seismology as a hydrological monitoring tool for rivers, even in the presence of strong**
 356 **cultural noise.**

357 **5 Conclusions**

358 This study investigated the passive seismic approaches to locate and characterize the seismic tremor induced by Avoca
 359 river, Co. Wicklow, Ireland. As this river located near a construction site and a busy local road and residential area, it
 360 was necessary to differentiate between the river-induced signal and the vibrations caused by cultural activity. We used
 361 beamforming array processing to locate the tremor in discrete frequency bands, observed as persistent signals on
 362 spectrograms. We could locate the persistent 8-17 Hz tremor on the first (upstream) and 10-23 Hz tremor on the second
 363 (downstream) array. Using FDPA, we observed that when wave types are not mixed, the tremor signal recorded by
 364 the stations in the arrays is Love wave dominated. The wave speed changes for the stations in the first array after 5:00
 365 A.M. which is the start of the daily human activity. This observation was in accordance with the dominance of
 366 Rayleigh wave components in the tremor on the stations after 5:00 A.M. based on FDPA analysis. When Rayleigh
 367 waves dominated the tremor, we could determine the direction of arrival based on the slope of the amplitude ratio
 368 between the horizontal components which gave consistent results compared to the BAZ calculated from the array
 369 processing. This shows that applying FDPA using a single 3C seismic station is a promising tool in the absence of
 370 seismic arrays. Finally, the observation of correlation between the median filtered seismic power integrated within the
 371 frequency range of the tremor and the river flow-rate demonstrated the capability of passive seismic as an indirect
 372 hydraulic monitoring tool, even in the presence of strong cultural noise.

373 **Acknowledgments**

374 We used the freely available software Obspy (Megies et al., 2011) for pre-processing seismic data and beamforming
 375 array analysis. We used MatLab for producing the median filtered spectrograms. We used the freely available code
 376 (Vore et al., 2019) for performing FDPA. We used the freely available software Geopsy (Wathelet et al., 2020) for
 377 analyzing HVSR. This project is part of the Geohazard spoke of the Irish Center for Research in Applied Geosciences
 378 (iCRAG) funded by the Science Foundation of Ireland (SFI). We acknowledge the Geological Survey Ireland (GSI)
 379 and Transport Infrastructure Ireland (TII) for financially supporting this project. We thank Wicklow County Council

380 for providing the site access to deploy seismic stations near Avoca River. We are very grateful to Dr. David Craig, for
381 his great assistance during the fieldwork.

382 **Open Research**

383 The raw seismic data used in this study is stored in the Dublin Institute for Advanced Studies (DIAS) data repository
384 and can be accessed by contacting the corresponding author. The water-level and flow-rate data can be freely
385 downloaded from the Environmental protection Agency (EPA) (<https://epawebapp.epa.ie/hydronet>). The
386 corresponding author of the paper can be contacted to access the codes used in this study.

387 **References**

- 388 Anthony, R.E., Aster, R.C., Ryan, S., Rathburn, S., Baker, M.G., 2018, Measuring Mountain River Discharge Using
389 Seismographs Emplaced Within the Hyporheic Zone, *Journal of Geophysical Research: Earth Surface*, 123, 1-19.
390
- 391 Bartholomaeus, T.C., Amundson, J.M., Walter, J.I., O'Neel, S., West, M.E., Larsen, C.F., 2015, Subglacial discharge
392 at tidewater glaciers revealed by seismic tremor, *Geophys. Res. Lett.*, 42, 6391–6398.
393
- 394 Burtin, A., Bollinger, L., Vergne, J., Cattin, R., Nabelek, J.L., 2008, Spectral analysis of seismic noise induced by
395 rivers: a new tool to monitor spatiotemporal changes in stream hydrodynamics, *J. Geophys. Res.* 113 (B5) B05301.
396
- 397 Burtin, A., Vergne, L.B.J., Cattin, R., Nabelek, J., 2011, Towards the hydrologic and bed load monitoring from high-
398 frequency seismic noise in a braided river: the 'torrent de st pierre', French Alps, *J. Hydrol*, 408 (1-2), 43–53.
399
- 400 Eibl, E.P.S., Bean, C.J., Einarsson, B., Palsson, F., Vogfjord, K.S., 2020, Seismic ground vibrations give advanced
401 early-warning of subglacial floods, *Nature Communications*, 2504, 1-11.
402
- 403 Gimbert, F., Tsai, V.C., Lamb, M.P., 2014, A physical model for seismic noise generation by turbulent flow in rivers,
404 *J. Geophys. Res. Earth Surf*, 119, 2209–2238.
405
- 406 Goodling, P.J., Lekic, V., Prestegard, K. 2018, Seismic signature of turbulence during the 2017 Oroville Dam
407 spillway erosion crisis, *Earth Surf. Dynam.*, 6, 351–367.
408
- 409 Govi, M., Maraga, F., Moia, F., 1993, Seismic detectors for continuous bed load monitoring in a gravel stream, *Hydrol.*
410 *Sci. J.*, 38, 123–132.
411
- 412 Hsu, L., Finnegan, N.J., Brodsky, E.E., 2011. A seismic signature of river bedload transport during storm events,
413 *Geophysical Research Letter*, 38 (13), L13407.
414
- 415 Larose E., 2015, Environmental seismology: What can we learn on earth surface processes with ambient noise?, 2015,
416 *Journal of Applied Geophysics*, 116, 62- 74.
417
- 418 Megies, T., Beyreuther, M., Barsch, R., Krischer, L. & Wassermann, J., 2011, ObsPy what can it do for data centers
419 and observatories?, *Ann. Geophys.*, 54, 4758.
420
- 421 Park, J., Vernon, F.L., Lindberg, C.R., 1987, Frequency Dependent Polarization Analysis of High-Frequency
422 Seismograms, *Journal of Geophysical Research*, 92(B12), 12664-12674.
423
- 424 Roth, D.L., Finnegan, N.J., Brodsky, Rickenmann, D., Turowski, J.M., Badoux, A., Gimbert, F., 2017, Bed load
425 transport and boundary roughness changes as competing causes of hysteresis in the relationship between river

426 discharge and seismic amplitude recorded near a steep mountain stream, *J. Geophys. Res. Earth Surf.*, 122, 1182-
427 1200.
428

429 Schmandt, B., Aster, R.C., Scherler, D., Tsai, V.C., Karlstrom, K.K., 2013, Multiple fluvial processes detected by
430 riverside seismic and infrasound monitoring of a controlled flood in the Grand Canyon, *Geophys. Res. Lett.*, 40, 4858-
431 4863.
432

433 Schmandt, B., Gaeuman, D., Stewart, R., Hansen, S.M., Tsai, V.C., Smith, J., 2017, Seismic array constraints on
434 reach-scale bedload transport, *Geology*, 45(4), 299-302.
435

436 Tsai, V.C., Minchew, B., Lamb, M.P., Ampuero, J.-P., 2012, A physical model for seismic noise generation from
437 sediment transport in rivers, *Geophysical Research Letters*, 39, L02404.
438

439 Vore, M.E., Bartholomaeus T.C., Winberry J.P., Walter J.I. and Amundson J.M., 2019, Seismic Tremor Reveals Spatial
440 Organization and Temporal Changes of Subglacial Water System, *Journal of Geophysical Research*, 124, 427- 446.
441

442 Wathelet, M., Chatelain, J.-L., Cornou, C., Di Giulio, G., Guillier, B., Ohrnberger, M. and Savvaidis, A., 2020,
443 Geopsy: A User-Friendly Open-Source Tool Set for Ambient Vibration Processing, *Seismological Research Letters*,
444 91(3), 1878- 1889.
445

446 Winberry, J.P., Anandakrishnan, S. and Alley, R.B., 2009, Seismic observations of transient subglacial water-flow
447 beneath MacAyeal Ice Stream, West Antarctica, *Geophysical Research Letter*, 36, L11502.
448